ELSEVIER

Biochimica et Biophysica Acta 1329 (1997) 85–96

BIOCHIMICA ET BIOPHYSICA ACTA
BBA

Phase behavior and permeability properties of phospholipid bilayers containing a short-chain phospholipid permeability enhancer

Jens Risbo [a], Kent Jørgensen [b], Maria M. Sperotto [a], Ole G. Mouritsen [a,*]

[a] *Department of Chemistry, Building 206, The Technical University of Denmark, DK-2800 Lyngby, Denmark*
[b] *Department of Pharmaceutics, The Royal Danish School of Pharmacy, Universitetsparken 2, DK-2100 Copenhagen Ø, Denmark*

Received 19 December 1996; revised 11 April 1997; accepted 17 April 1997

Abstract

The thermodynamic phase behavior and *trans*-bilayer permeability properties of multilamellar phospholipid vesicles containing a short-chain $DC_{10}PC$ phospholipid permeability enhancer have been studied by means of differential scanning calorimetry and fluorescence spectroscopy. The calorimetric scans of $DC_{14}PC$ lipid bilayer vesicles incorporated with high concentrations of $DC_{10}PC$ demonstrate a distinct influence on the lipid bilayer thermodynamics manifested as a pronounced freezing-point depression and a narrow phase coexistence region. Increasing amounts of $DC_{10}PC$ lead to a progressive lowering of the melting enthalpy, implying a mixing behavior of the $DC_{10}PC$ in the bilayer matrix similar to that of a substitutional impurity. The phase behavior of the $DC_{10}PC$–$DC_{14}PC$ mixture is supported by fluorescence polarization measurements which, furthermore, in the low-temperature gel phase reveal a non-monotonic concentration-dependent influence on the structural bilayer properties; small concentrations of $DC_{10}PC$ induce a disordering of the acyl chains, whereas higher concentrations lead to an ordering. Irreversible fluorescence quench measurements demonstrate a substantial increase in the *trans*-bilayer permeability over broad temperature and composition ranges. At temperatures corresponding to the peak positions of the heat capacity, a maximum in the *trans*-bilayer permeability is observed. The influence of $DC_{10}PC$ on the lipid bilayer thermodynamics and the associated permeability properties is discussed in terms of microscopic effects on the lateral lipid organization and heterogeneity of the bilayer. © 1997 Elsevier Science B.V.

Keywords: Lipid bilayer; Phase equilibrium; Short chain lipid; Permeability enhancer; Calorimetry; Fluorescence polarization; Bilayer heterogeneity

1. Introduction

Lipid vesicles consisting of closed shells of phospholipid bilayers have served a multitude of roles as model systems to study various functional and structural aspects of lipid organization that may be of relevance for both microscopic and macroscopic properties of the lipid bilayer component of biological membranes [1,2]. One of the key roles of the lipid-bilayer component of the cell membrane is to establish a physical barrier that protects the cell and

Abbreviations: DC_nPC, di-acyl-glycero phosphatidylcholine with *n* carbon atoms in each acyl chain; $DC_{10}PC$, didecanoyl phosphatidylcholine; $DC_{14}PC$, dimyristoyl phosphatidylcholine; $DC_{16}PC$, dipalmitoyl phosphatidylcholine; $DC_{18}PC$, distearoyl phosphatidylcholine; DSC, differential scanning calorimetry; NBD-PE, 7-nitrobenz-2-oxa-1,3-diazol-4-yl phosphatidyl ethanolamine; DPH, 1,6-diphenyl-1,3,5-hexatriene

* Corresponding author: Fax: (45) 4593-4808; E-mail: ogm@fki.dtu.dk

0005-2736/97/$17.00 © 1997 Elsevier Science B.V. All rights reserved.
PII S0005-2736(97)00091-6

prevents undesired transport of material across the membrane. In its capacity to form a self-assembled thin bimolecular capsule displaying unique barrier properties, the lipid bilayer constitutes the basic structural element responsible for maintaining a certain composition of organic and inorganic compounds in the cell interior that are vital for the cell functioning.

Although the lipid bilayer forms the physical boundary that separates and encapsulates the cytoplasm and the cell organelles, it is not a complete seal for the passive transport of molecular agents across the membrane [3]. In particular, it has become clear that a close relationship exists between, on the one hand the structural lipid bilayer behavior determined by the physicochemical conditions and on the other hand the associated functional barrier properties that control the passive transport of various molecular agents across the bilayer. The lipid bilayer constituents as well as the thermodynamic conditions imposed on the lipid bilayer by, e.g., temperature, hydrostatic pressure or ionic strength are all major determinants of the macroscopic phase behavior and bulk bilayer physical quantities [4]. Additionally, lipid bilayers display cooperative many-particle phenomena which on shorter length scales of 10–1000 Å can lead to the formation of a highly dynamic bilayer structure. This is reflected in terms of a lipid correlation length which can become rather large close to phase transitions and critical demixing points due to structural and compositional fluctuations of the many-particle lipid system [5,6]. The existence of a dynamic microstructure is, furthermore, of major importance as a key regulator of macroscopic bilayer properties such as the lateral area compressibility, the bilayer bending rigidity, and the passive diffusion of molecular compounds across the bilayer [2]. A large number of results from both experimental and theoretical investigations of well-defined lipid bilayer systems have clearly shown that the cooperative behavior of the many-particle lipid bilayer may be of paramount importance for a proper understanding of both functional and structural aspects of membrane processes [7–10].

A particularly striking correlation between the microscopic bilayer structure and the associated macroscopic properties of the lipid bilayer is the passive transport of material across the bilayer. In a by now classical experiment, it was demonstrated by Papahadjopoulus et al. [11] that phospholipid bilayers become extremely leaky in the temperature range of the gel-to-fluid transition. Monte Carlo computer simulations on a specific microscopic model have later shown that the anomaly in the passive diffusion of ions across the lipid bilayer at the gel-to-fluid main phase transition could be understood in terms of structural fluctuations and the appearance of leaky interfacial regions between dynamic coexisting gel and fluid clusters [12,13].

Various molecular compounds, such as cholesterol, peptides, and drugs incorporated into or interacting with lipid bilayers are able to change the heterogeneous microscopic lipid organization and the dynamic formation of lipid domains on various length and time scales [14]. For lipid bilayers incorporated with low cholesterol concentrations it has been shown that the lipid bilayer becomes more leaky, whereas higher cholesterol concentrations in the lipid bilayer lead to a decrease in the passive *trans*-bilayer permeation of small ions [15]. This observation is in accordance with the ability of cholesterol to increase the dynamic domain formation when present in low amounts in the bilayer [12]. In ideally behaving mixtures, such as $DC_{14}PC$–$DC_{16}PC$ mixtures, a recent study showed a close correlation between the leakiness of the lipid bilayer and the peak positions of the heat capacity curves which reflect the underlying structural fluctuations and the formation of dynamic coexisting lipid domains [16,17]. A related study of the effects of the insecticide lindane on the dynamic lipid bilayer microstructure and the associated permeability properties in the gel-to-fluid transition region demonstrated a sealing effect, although lindane at the same time increased the dynamic domain formation. This observation could be rationalized in terms of an accumulation of the small hydrophobic lindane molecules in the leaky interfacial bilayer regions appearing between dynamic coexisting gel and fluid lipid domains [18]. Obviously there is a need for further systematic studies of well-defined lipid bilayer systems that can provide detailed insight into the possible relationship between the dynamic lipid bilayer microstructure and the macroscopic physical lipid bilayer properties, such as the passive *trans*-bilayer permeability.

In particular, important drug-delivery aspects are related to an improved understanding of the relevant

barrier properties of the lipid bilayer component of biological membranes that controls the passive *trans*-membrane permeation of drug molecules to the sites of action. The use of permeability enhancers, which are able to change the lipid bilayer structure and the associated barrier properties exerted by the lipid bilayer, is a promising way for optimizing the pharmacological effects mediated by an increased drug concentration at the target sites [19]. Although permeability enhancers serve potential prospects as drug-delivery agents to promote the penetration of drugs through biological membranes, a detailed understanding of the underlying molecular effects exerted by drug delivery absorption enhancers on the lipid membrane physical structure is still lacking.

In this study, we have undertaken a systematic investigation of the influence of a short-chain $DC_{10}PC$ phospholipid absorption enhancer on the mixing behavior and permeability properties of lipid bilayers composed of $DC_{14}PC$. Both in vivo and in vitro studies have previously shown that the short-chain $DC_{10}PC$ lipid is an effective enhancer of the passive transport of pharmacological active compounds, such as hormones like insulin, across biological membranes [20]. Especially, the short-chain $DC_{10}PC$ lipid has been considered a promising candidate for improving parenteral peptide and protein delivery through the nasal epithelium which advantageously avoids first-pass hepatic metabolism and degradation of the labile macromolecules in the gastrointestinal tract [21].

2. Materials and methods

2.1. Materials and vesicle preparation

Fluorescent lipid probes NBD-PE and DPH were obtained from Molecular Probes (Eugene, OR). The $DC_{14}PC$ and $DC_{10}PC$ saturated phospholipids were purchased as powder from Avanti Polar Lipids (Birmingham, AL, USA) and were used without further purification. To form multilamellar binary lipid vesicles, weighed amounts of the phospholipids were dissolved in chloroform. Appropriate amounts of the NBD-PE and DPH probes were added to the chloroform solution to form lipid vesicles containing 0.5 mol% of the fluorescent probes. Chloroform was removed using a gentle stream of nitrogen leaving a thin lipid film which subsequently was dried overnight at low pressure to remove any trace impurities of the organic solvent. Multilamellar vesicles were made by dispersion of the dried lipid film in a 50 mM KCl and 1 mM NaN_3 solution. Lipid vesicles prepared for fluorescence assay bilayer permeability measurements were made by dispersion of the lipid film in a buffer solution containing 50 mM KCl, 1 mM NaN_3, and 20 mM HEPES (pH $\sim$ 7.5). The lipid suspension was kept for at least 1 h at ten degrees above the main transition temperature of $DC_{14}PC$. During this period, the lipid suspension was vortexed vigorously several times.

2.2. Differential scanning calorimetry

Differential scanning calorimetry of 10 or 20 mM multilamellar vesicles without the fluorescence probes incorporated was performed using a MicroCal MC-2 (Northhampton, MA) scanning calorimeter in the upscan mode at a scan rate of 10°C/h. The scans have been baseline corrected using a buffer vs. buffer scan whereas no correction of the heat capacity curves has been made for the fast time response of the power compensating calorimeter. Integration of the heat capacity curves in order to yield the transition enthalpy, ΔH, was performed using the Microcal Origin software. Phase boundaries were determined according to the method proposed by Mabrey and Sturtevant [22].

2.3. Fluorescence polarization measurements

Fluorescence polarization measurements were made with a SLM DMX-1100 fluorometer (SLM Instruments, Urbana, IL) in the T-format configuration. The polarization measurements of 0.5 mM multilamellar lipid samples incorporated with 0.5 mol% of the DPH fluorescent probe were obtained using 4 nm bandpaths for both the emission and excitation monochromators. The excitation and emission wavelengths for the DPH fluorescent probe were 336 and 450 nm, respectively. The lipid samples were placed in an improved thermostated cuvette holder controlled by an external water bath, and the temperature-dependent fluorescence polarization measurements were made in the upscan mode at a scan rate of 10°C/h. The temperature of the lipid

samples was measured with a thermistor inserted directly into the cuvette. The steady-state fluorescence polarization, *S*, was calculated as:

$$S = (I_{\parallel} - I_{\perp} G)/(I_{\parallel} + I_{\perp} G), \quad (1)$$

where $I_{\parallel}$ and $I_{\perp}$ are the parallel and perpendicular components of the emitted fluorescence intensities relative to the plane of the polarized excited light. *G* is a correction factor given by the ratio of sensitivities of the detection system for vertically and horizontally polarized light [23]. Single-point fluorescence polarization measurements were obtained using a time resolution of 10 s. The correction factor, *G*, was determined for each single point measurement.

2.4. Irreversible fluorescence quenching measurements

Permeability measurements of the multilamellar vesicles were based on the ability of dithionite, $S_2O_4^-$, to permeate lipid bilayers and irreversibly quench the head-group labeled fluorescent moiety of NBD-PE lipid analogs [24]. The excitation and emission wavelengths for the NBD-PE donor were 465 and 535 nm, respectively. A 2.5-ml aliquot of a 0.1-mM lipid suspension was placed in a thermostated cuvette and the time-dependent decay of the fluorescence intensity was monitored after the addition of 30 μl of a 1-M sodium dithionite solution freshly prepared using a 1-M Trizma (pH ~ 11) buffer stock solution. The thermostated lipid samples were equilibrated for 15 min prior to the addition of the irreversible dithionite quencher.

3. Results

3.1. Heat capacity

The heat capacity, C_p, obtained using differential scanning calorimetry for various composition of the $DC_{10}PC$–$DC_{14}PC$ mixture are shown in Fig. 1. The half-height width, $T_{1/2}$ ~ 0.03°C, for pure $DC_{14}PC$ is in accordance with values found in the literature for multilamellar vesicles [25]. As the concentration of the short-chain $DC_{10}PC$ lipid in the bilayer increases, a pronounced influence on the thermodynamic phase behavior is observed. This is most clearly seen as a concentration-dependent influence on the characteristic features of the heat capacity curves manifested as a broadening and shift of the peak positions towards lower temperatures. The broadening of the C_p curves reflects the thermodynamic phase behavior of the mixture and signals the existence of a gel–fluid phase-separated region. Based upon the characteristic features of the heat capacity curves [22], specifically the first and last extreme of the first derivative of the heat capacity, cf. curve D in Fig. 4a, the temperature span of the phase coexistence regions for the $DC_{10}PC$–$DC_{14}PC$ mixture has been estimated as marked by the heavy solid lines on the C_p curves in Fig. 1. The inserted figure shows the resulting estimated phase diagram for the $DC_{10}PC$–$DC_{14}PC$ mixture in the temperature and composition plane together with the full-scale C_p curves. It should be noted that the temperature range over which the mixture displays macroscopic phase coexistence only becomes slightly wider for increasing concentrations of $DC_{10}PC$. This behavior is noteworthy and may indicate unusual mixing properties of the short-chain $DC_{10}PC$ lipid in $DC_{14}PC$ lipid bilayers. Although a difference of four carbon atoms exists between the hydrocarbon acyl chains of the two lipid species, a

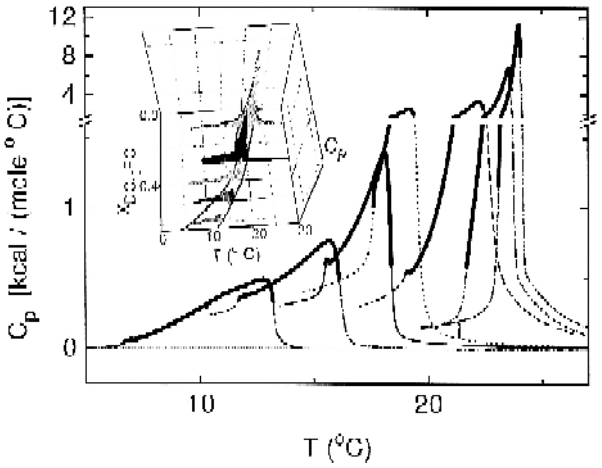

Fig. 1. Differential scanning heat capacity curves obtained at a scan rate of 10°C/h for $DC_{14}PC$ multilamellar vesicles incorporated with 1.5, 3, 10, 30, 40, 50, and 60 mol% $DC_{10}PC$ (curves from right to left). Notice the change in scale on the C_p axis. The position of the gel–fluid phase coexistence regions is indicated by heavy lines on the heat capacity curves. The insert shows the heat capacity curves in the temperature–composition plane for 10, 30, 40, 50, and 60 mol% $DC_{10}PC$. The underlying phase diagram for the $DC_{10}PC$–$DC_{14}PC$ mixture is indicated by heavy lines.

high degree of mixing is observed in contrast to the mixing behavior of longer chain saturated phospholipid mixtures, such as $DC_{14}PC$–$DC_{18}PC$ with the same chain-length difference which displays a fairly non-ideal mixing behavior [6,22]. We shall below return to a more detailed discussion of the mixing properties of the short-chain $DC_{10}PC$ lipid in longer chain host lipid bilayers.

Fig. 2 shows the melting enthalpy, ΔH, as a function of composition, $x_{DC_{10}PC}$, for the $DC_{10}PC$–$DC_{14}PC$ mixture. The ΔH values are determined as the areas under the part of the C_p curves marked with heavy solid lines in Fig. 1. The gel-to-fluid transition for pure $DC_{14}PC$ multilamellar vesicles takes place at 24.4°C and is characterized by a transition enthalpy of 5.5 kcal/mol in accordance with other published data [26]. As the concentration of $DC_{10}PC$ increases, a monotonous decrease of ΔH is observed similar to the influence of incorporating bulky stiff membrane compounds, such as cholesterol or small peptides into lipid bilayers [27,28]. To a first approximation, $DC_{10}PC$ therefore acts as substitutional impurity characterized by a rather limited internal flexibility compared to the host lipid which, due to plain entropy of mixing, gives rise to a concentration-dependent lowering of the melting enthalpy. This behavior is opposite to the influence of small solutes which act as interstitial impurities without any entropy of mixing and concomitant lowering of ΔH [18,25].

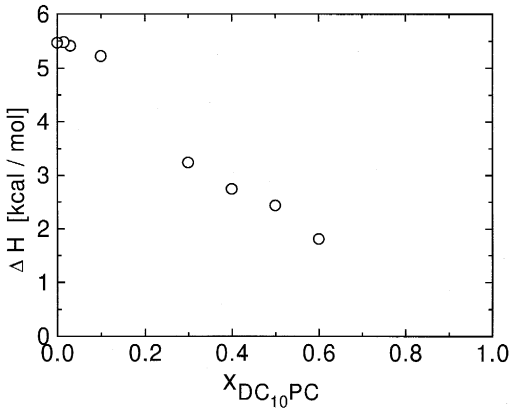

Fig. 2. The melting enthalpy, ΔH, per mol of total lipid as a function of composition, $x_{DC_{10}PC}$, for $DC_{14}PC$ multilamellar vesicles incorporated with 1.5, 3, 10, 30, 40, 50, and 60 mol% $DC_{10}PC$.

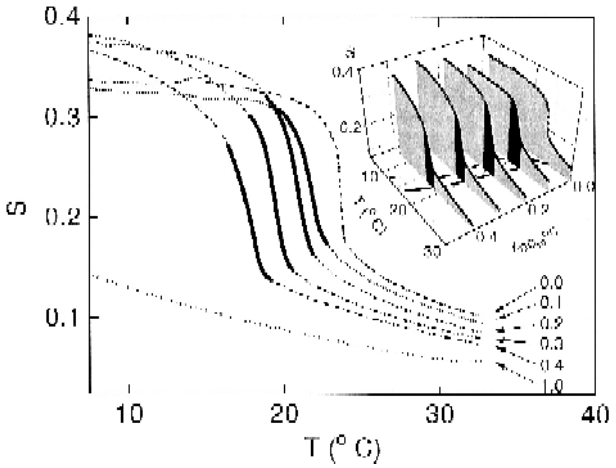

Fig. 3. Temperature-dependent DPH fluorescence polarization, S, for $DC_{10}PC$–$DC_{14}PC$ multilamellar vesicles containing 0, 10, 20, 30, 40, and 100 mol% $DC_{10}PC$. The position of the gel–fluid phase coexistence regions is indicated by heavy lines on the fluorescence polarization curves. The insert shows the polarization curves in the full temperature–composition plane. The underlying phase diagram is indicated by heavy lines.

3.2. Fluorescence polarization

To gain further insight into the microscopic changes of $DC_{14}PC$ lipid bilayers upon varying the molar fraction, $x_{DC_{10}PC}$, of the short chain lipid in the mixture, fluorescence polarization measurements were performed using DPH as a lipid bilayer incorporated probe. The temperature dependent DPH polarization, S, is shown in Fig. 3 for various concentrations of $DC_{10}PC$ in the $DC_{10}PC$–$DC_{14}PC$ mixture. For pure $DC_{14}PC$ multilamellar vesicles, a rather sharp change in S is observed when the multilamellar vesicles undergo the first-order gel-to-fluid chain-melting transition. The transition temperature of pure $DC_{14}PC$ vesicles, determined as the inflection point of S, is $T_m = 23.7$°C. The minor peak in the polarization curve at 14.3°C shows the position of the pretransition. As the concentration of $DC_{10}PC$ in the mixture increases a concomitant smearing and shift towards lower temperatures occur as reflected by the shape of S. The broadening and shift in temperature of the gel–fluid transition reported by the DPH polarization measurements are consistent with the calorimetric scans shown in Fig. 1. Moreover, both the spectroscopic and the thermodynamic measurements suggest the existence

of a rather narrow gel–fluid phase-separated region.

In the high-temperature fluid phase, a gradual lowering of the fluorescence polarization is observed for increasing amounts of $DC_{10}PC$ in the mixture. This effect indicates an apparent disordering of the acyl chains for higher concentrations of $DC_{10}PC$ even far away from the melting temperature, T_m, in contrast to the influence of other solutes. An example is certain drugs and insecticides, e.g., lindane that mainly affects the transitional behavior and the low-temperature gel phase, whereas no further disordering of the high-temperature fluid phase is observed [29]. Apparently, the decrease of S in the fluid phase indicates a global disordering of the fluid state $DC_{14}PC$ acyl chains as compared to the acyl chains in the pure $DC_{14}PC$ fluid phase. However, it should be noted that the DPH fluorescence polarization of pure $DC_{10}PC$ lipid bilayers is significantly lower than the corresponding values for both the $DC_{10}PC$–$DC_{14}PC$ mixtures and the pure $DC_{14}PC$ lipid bilayer. Therefore we are not in a position to exclude the possibility that the observed value of S reflects the location of DPH in different local bilayer environments, e.g., dynamic lipid domains that are enriched in either $DC_{10}PC$ or $DC_{14}PC$ lipids, respectively. Both experimental and theoretical investigations of local lipid structures in one-phase regions of binary lipid mixtures have clearly shown the existence of a highly heterogeneous lateral bilayer structure composed of dynamic lipid domains [6,30]. The location of DPH in local lipid structures could possibly be determined by invoking time-resolved fluorescence polarization measurements that enable detection of multiple fluorescence lifetimes corresponding to different rotational mobilities of the DPH probes in different local lipid bilayer environments. We shall return below to a discussion of the formation of heterogeneous local lipid structures and domains in binary mixtures which reside within thermodynamic one-phase regions that frequently and mistakenly are characterized as homogeneous one-phase regions.

In the low-temperature gel phase, the fluorescence polarization, S, demonstrates a non-monotonic concentration-dependent influence of $DC_{10}PC$ on the acyl chain conformational order. Small concentrations of $DC_{10}PC$, $x_{DC_{10}PC} = 0.1$, in the mixture give rise to a disordering of the acyl chain region, whereas higher concentrations, $x_{DC_{10}PC} = 0.2$, 0.3, and 0.4, induce an ordering of the bilayer core. It may well be that $DC_{10}PC$ in low concentrations in the gel phase acts as a simple impurity that induces a disordering of the bulk $DC_{14}PC$ bilayer matrix, whereas at higher concentrations, when the non-ideal mixing properties become more profound, an ordering of the acyl chains in the bilayer core takes place. Theoretical computer simulation calculations performed on binary lipid mixtures, such as $DC_{12}PC$–$DC_{18}PC$ or $DC_{14}PC$–$DC_{18}PC$ characterized by a high degree of non-ideality have demonstrated an increase in the acyl chain order parameters in the low-temperature gel phase [31,32].

The part of the polarization curves marked by heavy lines indicates the temperature ranges over which the $DC_{10}PC$–$DC_{14}PC$ mixtures display macroscopic gel–fluid phase coexistence. The more precise positions of the phase boundaries are established on the basis of the negative derivative of S, cf. Fig. 4b, with respect to temperature, $-dS/dT$, in analogy with phase diagrams based on thermodynamic response functions, e.g., heat capacity functions [22]. The phase diagram is indicated in the temperature–composition plane of the inserted three-dimensional representation of the polarization curves, $S(T)$, in Fig. 3. The phase diagram for the $DC_{10}PC$–$DC_{14}PC$ mixture estimated on basis of the calorimetric data and the fluorescence data, cf. Figs. 1 and 3, demonstrates a good agreement between the two different and independent experimental techniques. In particular, the consistency between the spectroscopic and the thermodynamic results becomes clear by inspection of Fig. 4a, which enables a detailed comparison between the calorimetric and fluorescence results for a selected composition, $x_{DC_{10}PC} = 0.4$, of the $DC_{10}PC$–$DC_{14}PC$ mixture. The upper curve (A) in Fig. 4a shows the DPH fluorescence polarization, S, whereas curve B shows $-dS/dT$. There is a remarkable similarity between the temperature dependence of $-dS/dT$ (curve B) and the heat capacity, C_p (curve C). Both curves display the same transitional characteristics manifested as a rather abrupt change when the phase coexistence region is approached from the high-temperature fluid phase. This is followed by a slowly descending curve towards the low-temperature gel phase. Moreover both curves suggest the existence of a rather narrow gel–fluid phase separated region located between 15.5 and

19.2°C. Fig. 4b shows the partial phase diagram for the $DC_{10}PC$–$DC_{14}PC$ mixture estimated on basis of both the calorimetric and the spectroscopic data.

3.3. Permeability

In an attempt to relate the effects of $DC_{10}PC$ on the structural behavior of the lipid bilayer due to changes in functional bilayer properties, such as the passive *trans*-bilayer permeability, we have performed a series of irreversible fluorescence quench experiments at selected positions in the phase diagram as marked by asterisks in Fig. 4b. When dithionite is added to the outer aqueous phase of multilamellar lipid bilayers incorporated with NBD-PE head-group labeled lipids, an irreversible time-dependent reduction of the fluorescence signal is observed. The time-dependent decrease of the fluorescence signal is determined by the barrier properties of the lipid bilayers and the ability of the dithionite quenching agent to get into contact with NBD-PE lipids positioned in the inner core of the multilamellar vesicles. Fig. 5 illustrates the time development of the normalized fluorescence signal for $DC_{10}PC$–$DC_{14}PC$ mixtures at selected temperatures and compositions. Immediately after the addition of dithionite to the lipid sample a rapid decrease of the fluorescence to a value of 90% takes place. The fast reduction corresponds to a quenching of the head-group labeled NBD-PE lipids positioned in the outermost leaflet of the multilamellar vesicles. This is

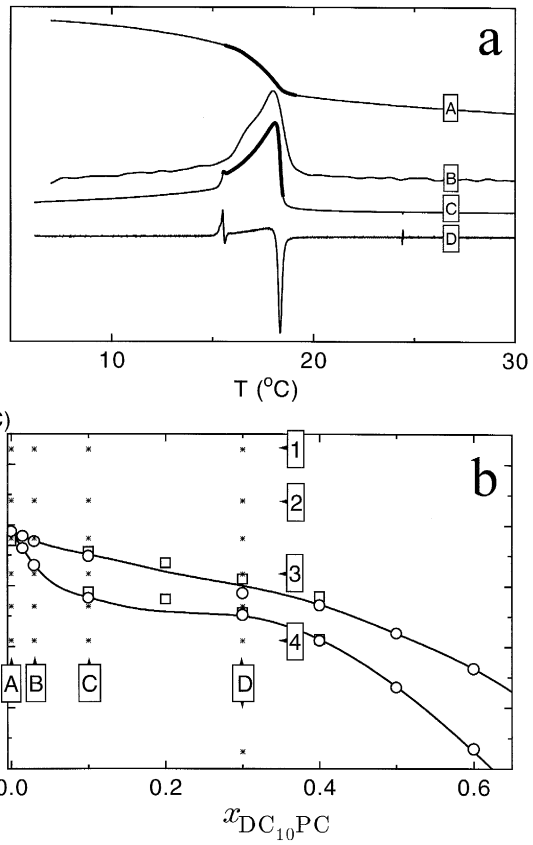

Fig. 4. a: comparison of DPH fluorescence polarization and heat capacity data for $DC_{10}PC$–$DC_{14}PC$ lipid vesicles incorporated with 40 mol% $DC_{10}PC$. A, DP polarization, S, as a function of temperature. The approximate location of the coexistence regions is marked with a heavy line; B, the negative derivative of the DPH fluorescence polarization, $-dS/dT$; C, heat capacity, C_p; and D, first derivative of the heat capacity, dC_p/dT. b: phase diagram of $DC_{10}PC$–$DC_{14}PC$ multilamellar lipid vesicles estimated on basis of C_p curves (◦) as described in the text, and on the basis of the negative derivative of the DPH fluorescence polarization, $-dS/dT$ (□). The solid lines indicate the position of the solidus and liquidus phase boundaries. The locations in the phase diagram marked by asterisks correspond to compositions and temperatures for the permeability experiments.

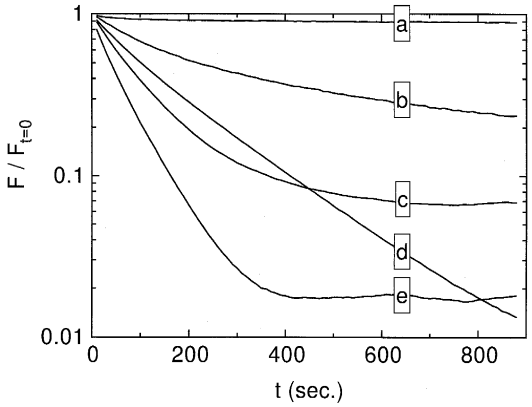

Fig. 5. Fluorescence intensity, F, as a function of time after the addition of the irreversible dithionite quencher to multilamellar $DC_{10}PC$–$DC_{14}PC$ lipid vesicles incorporated with 0.5 mol% fluorescent NBD-PE. The time-dependent fluorescence intensity is normalized with respect to the stable fluorescence intensity, $F_{t=0}$, prior to the addition of the irreversible dithionite quencher. a, $x_{DC_{10}PC} = 0.03$ and $T = 31.3$°C; b, $x_{DC_{10}PC} = 0.03$ and $T = 23.0$°C; c $x_{DC_{10}PC} = 0.10$ and $T = 18.3$°C; d, $x_{DC_{10}PC} = 0.30$ and $T = 6.4$°C; and e, $x_{DC_{10}PC} = 0.30$ and $T = 18.3$°C. Notice that the normalized fluorescence intensity, $F/F_{t=0}$, is shown on a logarithmic scale.

followed by a slow time-dependent decrease which is strongly influenced by both temperature and composition of the lipid mixture as seen in Fig. 5. In the high-temperature fluid phase, $T = 31.3$°C, a low concentration of $DC_{10}PC$, $x_{DC_{10}PC} = 0.03$ (Fig. 5a), leads to a slow reduction of the fluorescence intensity whereas lowering of temperature to 23.0°C (Fig. 5b), close to the position of the liquidus phase boundary, results in a more pronounced fast reduction of the fluorescence. In the low-temperature gel phase, the time traces of the fluorescence signals demonstrate a more dramatic enhancement of lipid bilayer leakiness. At $T = 18.3$°C and $x_{DC_{10}PC} = 0.10$ (Fig. 5c) a rapid decay is observed. The low-temperature leakiness becomes even more pronounced when the concentration is increased to $x_{DC_{10}PC} = 0.30$ (Fig. 5e). At $T = 6.4$°C and $x_{DC_{10}PC} = 0.30$ (Fig. 5d) the fluorescence decrease is characterized by a slightly weaker initial change followed by a significant long-term change. The unusual low-temperature effect is a possible manifestation of low-temperature phase separation and the existence of a lower critical demixing point. If the lipid mixture displays low-temperature phase coexistence or is positioned in the vicinity of a critical demixing point, the interpretation of the time-dependent decay of the fluorescence intensity becomes even more complicated since an accumulation of NBD-PE lipids in $DC_{14}PC$ enriched bilayer regions can lead to a self-quenching of the NBD fluorescent moieties [33].

Obviously, the time-dependent decay of the fluorescence intensities presented in Fig. 5 cannot be analyzed according to a single exponential, as suggested by Langner and Hui, for pure lipid bilayers [24]. Instead of invoking a multi-exponential fitting procedure that does not provide further details of the molecular mechanisms involved, the normalized fluorescence after 200 s, P_{200}, has been chosen as a relevant quantity that enables a qualitative comparison of the barrier properties exerted by the $DC_{10}PC$–$DC_{14}PC$ lipid bilayers at different temperatures and compositions. A low value of P_{200} implies a high permeability. Fig. 6 shows P_{200} as a function of $DC_{10}PC$ concentration for four different temperatures, $T = 31.3$, 26.7, 23.9, and 15.5°C. In the high-temperature fluid phase, $T = 31.3$°C (Fig. 6, 1), a small decrease in P_{200} is observed whereas at $T = 26.7$°C (Fig. 6, 2) increasing amounts of $DC_{10}PC$ lead to a more permeable bilayer structure. In the low-temperature gel phase, $T = 15.5$°C, (Fig. 6, 4) a rapid concentration dependent decline of P_{200} is observed resulting in an extremely leaky lipid bilayer. At $T = 23.9$°C (Fig. 6, 3) the P_{200} curve displays a minimum in the neighborhood of the gel–fluid phase separated region as marked by the heavy solid line. Fig. 7 shows the temperature dependence of P_{200} at different compositions of the $DC_{10}PC$–$DC_{14}PC$ mixture. For pure $DC_{14}PC$ multilamellar vesicles the well-known temperature anomaly of the *trans*-bilayer permeability is observed at the gel-to-fluid transition [11]. When the concentration of $DC_{10}PC$ in the lipid mixture increases, a remarkable enhancement of the leakiness of lipid bilayer is detected over broad temperature ranges. In the low-temperature one-phase gel region, a dramatic increase in the *trans*-bilayer permeability is observed, whereas a much weaker effect is present in the one-phase fluid regions. The temperature scans in Fig. 7 reveal a maximum in the leakiness of the $DC_{10}PC$–$DC_{14}PC$ lipid mixtures at temperatures corresponding to the peak positions of

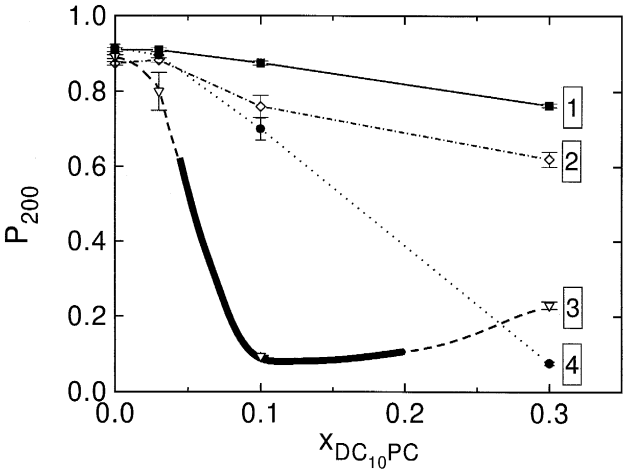

Fig. 6. Fluorescence intensity, $P_{200} = F_{t=200} / F_{t=0}$, as measured 200 s after the addition of the irreversible dithionite quencher to $DC_{10}PC$–$DC_{14}PC$ lipid vesicles incorporated with 0.5 mol% fluorescent NBD-PE, as a function of composition, $x_{DC_{10}PC}$, for different temperatures marked in the phase diagram shown in Fig. 4b. 1, $T = 31.3$°C; 2, $T = 26.7$°C; 3, $T = 23.9$°C; and 4, $T = 15.5$°C. The fluorescence intensity is normalized with respect to the stable fluorescence intensity prior to the addition of the irreversible dithionite quencher.

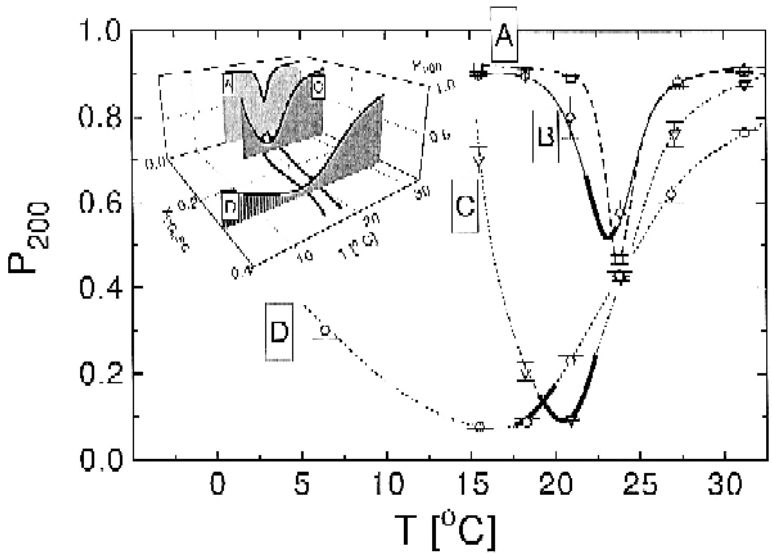

Fig. 7. Fluorescence intensity, $P_{t=200}$, as measured 200 s after the addition of the irreversible dithionite quencher to $DC_{10}PC$–$DC_{14}PC$ lipid vesicles incorporated with 0.5 mol% fluorescent NBD-PE, as a function of temperature, T, for different compositions marked in the phase diagram shown in Fig. 4b. A, $x_{DC_{10}PC} = 0$; B, $x_{DC_{10}PC} = 0.03$; C, $x_{DC_{10}PC} = 0.10$; and D, $x_{DC_{10}PC} = 0.30$. The fluorescence intensity is normalized with respect to the stable fluorescence intensity prior to the addition of the irreversible dithionite quencher. The insert shows a three-dimensional representation of $P_{t=200}$ as a function of temperature, T, and composition, $x_{DC_{10}PC}$. The heavy solid lines in the temperature and composition plane mark the positions of the solidus and liquidus phase boundaries.

the heat capacity curves, i.e., in the coexistence region, cf. Fig. 1.

4. Discussion and conclusion

The effects of the short-chain $DC_{10}PC$ permeability enhancer on the thermodynamic phase behavior of a $DC_{14}PC$ host lipid bilayers have been investigated by DSC and fluorescence polarization spectroscopy. A qualitative different mixing behavior is observed for this binary mixtures as compared to mixtures of lipids with longer chains characterized by the same degree of mismatch between the hydrophobic acyl chains [22]. Preliminary DSC data on mixtures of $DC_{10}PC$ and $DC_{16}PC$ (Christiansen et al., unpublished) support this observation, although the gel–fluid phase coexistence region as expected is broader (reflecting the more non-ideal mixing behavior in this mixture) possibly bounded by a three-phase line suggesting immiscibility of the gel phases. Increasing amounts of $DC_{10}PC$ in $DC_{14}PC$ lead to a broadening of the transition followed by a lowering of the transition enthalpy. Such findings indicate that the short-chain lipid acts as a simple substitutional bilayer impurity characterized by limited flexibility of the hydrophobic acyl chains compared to the acyl chains of the host lipid. Associated effects on the physical lipid bilayer properties, such as the passive *trans*-bilayer permeability, were determined using irreversible fluorescence quench measurements. The results reported above demonstrate a pronounced influence of the short-chain phospholipid on the structural phase behavior and the associated barrier properties of the mixture. This suggests the case of a lipid bilayer which becomes more leaky over broad temperature and compositions ranges. In particular, a dramatic increase in the leakiness of the lipid bilayer is found in the one-phase gel region whereas a less pronounced effect is observed in the one-phase fluid region. A maximum in the *trans*-bilayer permeability is observed at temperatures corresponding to the peak position of the heat capacity curves.

Our study shows that $DC_{10}PC$ can be incorporated into longer chain phospholipid host bilayers in very large quantities without disrupting the bilayer structure. In fact, liposomes can be produced by pure $DC_{10}PC$ [34,35] which is supported by our finding

that lipid preparations of pure $DC_{10}PC$ incorporated with head-group labeled NBD-PE lipids can only be incompletely quenched by dithionite in accordance with the existence of lipid aggregates with one side being shielded from the quencher (Risbo et al., unpublished).

Our combined calorimetry and fluorescence polarization data suggest the phase equilibria for $DC_{10}PC$–$DC_{14}PC$ and $DC_{10}PC$–$DC_{16}PC$ mixtures to be rather similar. It should be remarked, however, that these techniques only lead to an approximate and incomplete phase diagram because they provide information on second derivatives of the free energy only. This is particularly cumbersome if, as in the present case, the lipid bilayers are subject to strong fluctuations in the transition region [32] and where it is possible that there may be critical mixing points or critical endpoints in the phase diagram. Indeed it is possible that the lower right-hand side of the phase diagram in Fig. 4b is misleading, and that the diagram rather should be closed with an endpoint. The high permeability and wide wings in the heat capacity observed in this region may then reflect the extreme density and compositional fluctuations that are expected in a large region around such a point, in analogy with what has been found for mixtures of $DC_{16}PC$ and *trans*-bilayer amphiphilic peptides [28]. A schematic illustration of the type of lateral bilayer organization one should expect in this region is given in Fig. 8 which shows results obtained from computer-simulation calculations on a microscopic model of lipid bilayers that have been used successfully to study microscopic properties of binary lipid mixtures [6]. The model builds upon the conformational statistics of the acyl chains and treats the bilayer as uncoupled monolayers. A detailed description of the model can be found in [5]. It is possible that the wide wings in the heat capacity observed at low temperatures for the mixtures with high concentrations of $DC_{10}PC$, cf. Fig. 1, are caused by such density and compositional fluctuations.

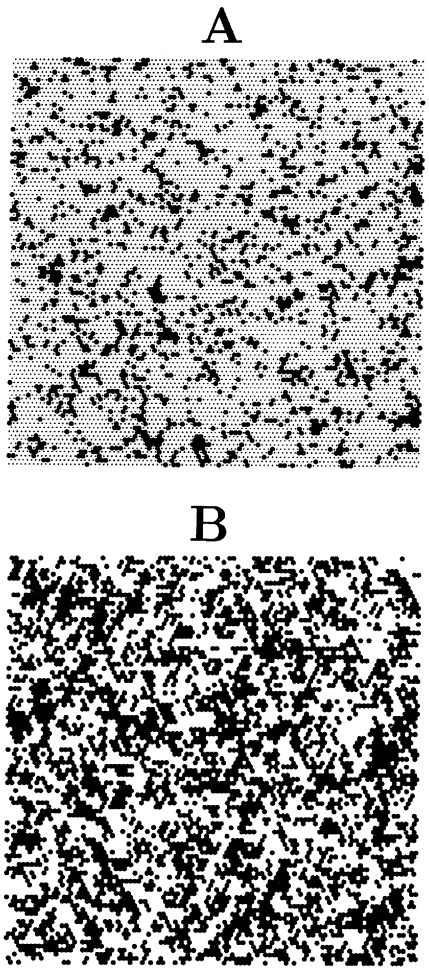

Fig. 8. Lateral lipid bilayer structure at $T = 32°C$ of a pure $DC_{14}PC$ lipid bilayer in the fluid phase (A) and a $DC_{10}PC$–$DC_{14}PC$ lipid mixture at $x_{DC_{10}PC} = 0.45$ in the thermodynamic one-phase gel (fluid) regions of its phase diagram (B). The lateral heterogeneity in A reflects density fluctuations with small gel-like (black) dynamic clusters in a bulk fluid bilayer. The lateral heterogeneity in B reflects the compositional fluctuations in the fluid phase where the two lipid species are indicated in black and white. The lipid bilayer configurations are obtained from Monte Carlo computer simulations on lipid systems corresponding to 5000 lipid molecules. For details of the simulations, see Jørgensen et al. [6].

Strong fluctuations, in particular density fluctuations, not only lead to large values and peaks in the heat capacity. Enhanced passive permeability of lipid bilayers is also expected to be a consequence of bilayer fluctuations [36]. Peaks in the permeability are therefore expected qualitatively to track peaks in the heat capacity. The reason for this has been proposed to be the lateral dynamic heterogeneity, cf. Fig. 8, which entails a substantial amount of defects and defect lines in the bilayer which are assumed to be leaky regions [36]. This relation between heat capacity and permeability has been found to hold for pure lipids [36] as well as for lipid mixtures, e.g., for

$DC_{14}PC$–$DC_{16}PC$, where a broad peak in both the heat capacity and the permeability is observed across the phase coexistence region [16], and for $DC_{14}PC$–$DC_{18}PC$ where two resolved heat capacity peaks signaling the phase boundaries of the coexistence region have recently been shown to be accompanied by two corresponding peaks in the permeability (Sparre Andersen et al., unpublished). For the present mixtures with $DC_{10}PC$, only a single heat capacity peak can be resolved, cf. Fig. 1, and consistent with the above, a permeability peak is found to track to heat capacity peak, cf. Fig. 7. The packing defects mentioned above as mediators for the permeation may be especially pronounced in mixtures containing a short-chain lipid, like $DC_{10}PC$, because the short chains, due to their limited internal flexibility relative to longer ones, would adapt less easily to the defect lines and therefore lead to more leaky regions.

The increased permeability of lipid bilayers incorporated with the short-chain $DC_{10}PC$ lipid is consistent with the results of a recent small-angle neutron scattering study of the swelling properties of $DC_{14}PC$ multilamellar bilayers incorporated with small amounts of $DC_{10}PC$ [37]. This study showed that the anomalous swelling behavior at the transition was enhanced by $DC_{10}PC$. This was interpreted as an indication of a lowering of the bilayer bending rigidity due to $DC_{10}PC$'s ability to enhance the fluctuations of the lipid bilayer system.

A study of permeability properties of binary lipid mixtures in their coexistence region may be complicated by the fact that mixtures involving species with different acyl-chain lengths may to be subject to an extremely slow phase separation dynamics that proceeds on a time scale of hours [31,38]. We have at present no information available about the relevant time scale for the demixing of the mixtures studied in the present paper and whether this scale influences the permeability. For the $DC_{10}PC$–$DC_{14}PC$ mixture, a time-dependent decrease of the NBD-PE fluorescence was observed for pure $DC_{10}PC$ bilayers even without adding dithionite to the lipid vesicles (Risbo et al., unpublished). This may be a possible manifestation of the poor mixing properties of the long-chain NBD-PE fluorescent probe in the $DC_{10}PC$ lipid matrix. As a consequence, a two-dimensional dynamic phase separation process is expected to take place [31] resulting in a certain amount of self-quenching of the fluorescent moieties in NBD-PE enriched regions.

The effects of adding $DC_{10}PC$ to a lipid-bilayer host with longer acyl chains in terms of acyl-chain order are highly non-trivial. As shown in Fig. 3, increasing amounts of $DC_{10}PC$ added to the fluid phase lead to decreased order in the acyl chains of $DC_{14}PC$ (measured by the fluorescence polarization). However, in the low-temperature phase, the effect on the acyl-chain order is non-monotonic, first decreasing and subsequently increasing the order as a function of added amounts of $DC_{10}PC$. We have no simple explanation for this unexpected result which may indicate that the phase equilibria at low temperatures could be more complex than suggested by the phase diagram in Fig. 4b.

$DC_{10}PC$ has been proposed as an enhancer of *trans*-membrane transport. Specifically, it has been shown to enhance the permeation of various substances, such as insulin [20] and ions across rabbit nasal airway epithelium partly due to structural changes in the tight junctions and the physicochemical properties of the lipid bilayer part of the cell membrane [39]. In vivo studies of the uptake and metabolism after nasal application of $DC_{10}PC$ showed a very rapid hydrolysis within the first minutes due to degradation by phospholipases [40]. These results indicate that the molecular mechanisms involved in the observed in vivo enhancer effect of $DC_{10}PC$ can partly be mediated by the hydrolysis products, e.g., fatty acids. Systematic permeability studies along the lines of the present paper carried out on well-defined lipid systems incorporated with various amounts of the hydrolysis products may help clarify to which extent the short-chain $DC_{10}PC$ lipid or the hydrolysis products are involved in the observed in vivo enhancer effect.

Acknowledgements

This work was supported by the Danish Natural Science Research Council and the Danish Technical Research Council. The authors' interest in short-chain phospholipid permeability enhancers was stimulated via discussions with Dr. Ole Frederiksen. O.G.M. is an Associate fellow of the Canadian Institute for Advanced Research.

References

[1] R.B. Gennis, Biomembranes. Molecular Structure and Function, Springer-Verlag, London, 1989.
[2] M. Bloom, E. Evans, O.G. Mouritsen, Q. Rev. Biophys. 24 (1991) 293–397.
[3] E.A. Disalvo, S.A. Simon (Eds.), Permeability and Stability of Lipid Bilayers, CRC Press, Boca Raton, FL, 1994.
[4] P.K.J. Kinnunen, P. Laggner, Chem. Phys. Lipids 57 (1991) 109–408.
[5] O.G. Mouritsen, in: R. Brasseur (Ed.), Molecular Description of Biological Membrane Components by Computer Aided Conformational Analysis, Vol. 1, CRC Press, Boca Raton, FL, 1990, pp. 3–83.
[6] K. Jørgensen, M.M. Sperotto, O.G. Mouritsen, J.H. Ipsen, M.J. Zuckermann, Biochim. Biophys. Acta 1152 (1993) 135–145.
[7] E. Sackmann, FEBS Lett. 346 (1994) 3–16.
[8] O.G. Mouritsen, K. Jørgensen, Bioessays 14 (1992) 129–136.
[9] O.G. Mouritsen, K. Jørgensen, Chem. Phys. Lipids 73 (1994) 3–25.
[10] P.K.J. Kinnunen, O.G. Mouritsen, Chem. Phys. Lipids 73 (1994) 1–236.
[11] D. Papahadjopoulos, K. Jacobsen, S. Nir, T. Isac, Biochim. Biophys. Acta 311 (1973) 330–348.
[12] L. Cruzeiro-Hansson, O.G. Mouritsen, Biochim. Biophys. Acta 944 (1988) 63–72.
[13] O.G. Mouritsen, K. Jørgensen, Mol. Membr. Biol. 12 (1995) 15–20.
[14] L.O. Bergelson, K. Gawrisch, J.A. Ferretti, R. Blumenthal (Eds.), Special Issue on Domain Organization in Biological Membranes, Mol. Membr. Biol. 12 (1995) 1–162.
[15] E. Corvera, O.G. Mouritsen, M.A. Singer, M.J. Zuckermann, Biochim. Biophys. Acta 1107 (1992) 261–270.
[16] G.S. Clerc, T.T. Thompson, Biophys. J. 68 (1996) 2333–2341.
[17] E. Freire, R.L. Biltonen, Biochim. Biophys. Acta 514 (1978) 54–68.
[18] M.C. Sabra, K. Jørgensen, O.G. Mouritsen, Biochim. Biophys. Acta 1282 (1996) 85–92.
[19] V.H.L. Lee, J. Control. Release 13 (1990) 69–97.
[20] S. Carstens, G. Danielsen, B. Guldhammer, O. Frederiksen, Diabetes 42 (1993) 1032–1040.
[21] X.H. Zhou, J. Control. Release 29 (1994) 239–252.
[22] S. Mabrey, J.M. Sturtevant, Proc. Natl. Acad. Sci. USA 73 (1976) 3862–3866.
[23] J.R. Lakowicz, Principles of Fluorescence Spectroscopy, Plenum Press, New York, 1983.
[24] M. Langner, S.W. Hui, Chem. Phys. Lipids 65 (1992) 23–30.
[25] M.C. Sabra, K. Jørgensen, O.G. Mouritsen, Biochim. Biophys. Acta 1233 (1995) 89–104.
[26] D. Marsh, Handbook of Lipid Bilayers, CRC Press, Boca Raton, FL, 1990.
[27] J.H. Ipsen, O.G. Mouritsen, M.J. Zuckermann, Biophys. J. 56 (1989) 661–667.
[28] Z. Zhang, M.M. Sperotto, M.J. Zuckermann, O.G. Mouritsen, Biochim. Biophys. Acta 1147 (1993) 154–160.
[29] M.C. Antunes-Madeira, V.M.C. Madeira, Biochim. Biophys. Acta 982 (1989) 161–166.
[30] W. Knoll, K. Ibel, E. Sackmann, Biochemistry 20 (1981) 6379–6383.
[31] K. Jørgensen, O.G. Mouritsen, Biophys. J. 69 (1995) 942–954.
[32] J. Risbo, M.M. Sperotto, O.G. Mouritsen, J. Chem. Phys. 103 (1995) 3643–3656.
[33] K. Hong, P.A. Baldwin, T.M. Allen, D. Papahadjopoulos, Biochemistry 27 (1988) 3947–3955.
[34] B.A. Lewis, D. Engelman, J. Mol. Biol. 166 (1983) 211–217.
[35] R.N.A.H. Lewis, N. Mak, R.N. McElhaney, Biochemistry 26 (1987) 6118–6126.
[36] O.G. Mouritsen, K. Jørgensen, T. Hønger, in: E.A. Disalvo, S.A. Simon (Eds.), Permeability and Stability of Lipid Bilayers, CRC Press, Boca Raton, FL, 1994, pp. 137–160.
[37] J. Lemmich, T. Hønger, K. Mortensen, J.H. Ipsen, R. Bauer, O.G. Mouritsen, Eur. Biophys. J.: Biophys. Lett. 25 (1996) 61–65.
[38] K. Jørgensen, A. Klinger, M. Braiman, R.L. Biltonen, J. Chem. Phys. 100 (1996) 2766–2769.
[39] M. Röpke, M. Hansen, S. Carstens, P. Christensen, G. Danielsen, O. Frederiksen, Am. J. Physiol. 271 (1996) L646–L655.
[40] C. Vermehren, P.B. Johansen, H.S. Hansen, Drug Metab. Dispos., in press.